Journal of Mines, Metals and Fuels, *71(12C) : 494-505; 2023. DOI: 10.18311/jmmf/2023/47316*

Print ISSN : 0022-2755

Journal of Mines, Metals and Fuels

Contents available at: *www.informaticsjournals.com/index.php/jmmf*

Quantum Chemical Computations, Photophysical Properties and Molecular Docking of Coumarin Derivative

P. Bhavya[1*], T. M. Mohan Kumar[2], Raviraj Kusanur[3], P. A. Dinesh[4] and Vijaya Kumar[4]

[1]Department of Physics, New Horizon College of Engineering, Bangalore - 560103, Karnataka, India
bhavyap26@gmail.com
[2]Department of Chemistry, Amrita School of Engineering, Amrita Vishwa Vidyapeetham
Bengaluru - 560035, India
[3]Department of Chemistry, R.V. College of Engineering, Bangalore - 560059, Karnataka, India
[4]Department of Mathematics, M. S. Ramaiah Institute of Technology, Bangalore - 560054, Karnataka, India

Abstract

This research utilises a combination of computational and experimental methods to examine the spectral and photophysical characteristics of the coumarin derivative [1-Methyl-benzo[f]chromen-3-one (1MBC)]. The ground and excited state dipole moments are calculated using various polarity and polarizability solvents. With increasing solvent polarity, an increase in wavelength was seen, indicating a π →π* transition caused by intermolecular charge transfer interactions. Additionally, experimentally measured dipole moment (Δμ) values are compared to microscopic empirical solvent polarity values. Density Functional Theory (DFT) calculations employing B3LYP/6-31+G (d, p) basis sets were utilised to explore molecular properties via quantum chemical simulations, along with conducting Frontier Molecular Orbitals (FMO) analysis to study chemical reactivity and kinetic stability. The properties of Mulliken charges and Non-Liner Opticals (NLOs) are investigated further. Natural Bond Orbital (NBO) analysis reveals a substantial stabilisation energy, indicating a specific donor-acceptor interaction via proton transfer. The software Schrodinger Maestro 11.2 was utilised to carry out docking studies. The binding affinities of 1MBC with periplasmic protein were determined using the GLIDE scores (PDB ID-2IPM). The spectroscopic and quantum computational work presented here is critical for using boronic acid derivatives as chemo sensors and the rational design of novel molecular probes. Heterocyclic organic compounds such as which contain at least one ring with atoms of at least two different elements such as Coumarin derivatives, have various applicability in the mining field such as corrosion inhibitors in equipment, flotation agents etc.

Keywords: Corrosion Inhibitors, DFT Studies, Dipole Moments, Fluorescence, Fuel Additives, Quantum Chemical Computations

1.0 Introduction

With the advancement of modern science and technology, researchers have been able to examine the nature of life activities in greater depth thanks to fluorescent molecules for providing non-invasive, selective and sensitive research tools. The family of Coumarin derivatives are one of such fluorescent probes that are being explored as an active class of dyes known for their potential application in diverse fields of science and technology

Author for correspondence

such as fluorescence imaging, chemo sensing[1], biomedical engineering, chemical biology[2], synthetic, organic chemistry[3], materials and bioorganic chemistry[4,5]. Owing to the wide pharmaceutical and biochemistry applications, including the fields of mines, minerals and fuels, the spectroscopic investigations of these compounds have become a pressing need of the time. Also, derivatives of coumarins can be applied as corrosion inhibitors to shield metals from rust and other deterioration[6]. This is crucial since metals in the mining sector are subjected to hostile conditions.

Various fluorescent spectroscopic methods like solvatochromic method[7], rotational dynamic studies[8], quenching studies[9,10] and DFT studies[11] are some most commonly used techniques. Knowledge of dipole moments opens the window to understanding molecular geometry[12]. This is extremely useful when building new molecules for NLO applications[13]. DFT calculations present beneficial information on contributes to the advancement of novel medicinal compounds and enhances comprehension of the correlation between biological systems and material science[15].

The dipole moments of the Coumarin derivative 1MBC are investigated theoretically and experimentally, using solvatochromic and DFT/B3LYP methods respectively. The optimised molecular structure along with the integrated electronic density mapped with the Molecular Electrostatic Potential (MEP), NBO, FMO and NLO properties are all explored using the Gaussian 09 program. As these compounds can also be used in sensing applications, their interactions with amino acid residues of periplasmic proteins of the blood can also be studied by docking.

2.0 Materials and Methods

2.1 Materials

Laboratory synthesis was done for 1-Methyl-benzo[f] chromen-3-one (1MBC) using standard methods[16] and Figure 1 presents the molecular structures of 1MBC. The solvents were procured from S-D-Fine Chemicals Ltd. Molecular docking studies for the sample were performed using the crystal structure of the galactose-binding periplasmic protein (PDB ID: 2IPM and 2IPL), obtained from the Protein Data Bank, utilised for preparing the docking samples using the Protein Preparation Wizard[17].

2.2 Dipole Moments Through Empirical Formula

The several solvatochromic equations that are used to calculate the dipole moments are credited to Bilot and Kawski, Lippert, Bkhshiev, Kawski-Chamma-Viallet and Reichardt[18-22]. Literature values from these papers were used for calculations.

2.3 Computation Using Quantum Chemistry

The 6-31+G (d, p) basis set via Gaussian 09 W[23] is used for the sample in the DFT/B3LYP approach for quantum chemical calculations. Theoretical dipole moments were computed in the gas phase. Using Gauss View 5.0 and gradient geometry optimisation, the geometry of the compound was fully optimised[24]. NBO computation was done with NBO version 5.0[25].

3.0 Results and Discussion

3.1 Photophysical Behavior Analysis

3.1.1 Effect of Solvent on Spectra

Absorption spectra of 1MBC show peaks around 353-359nm. The position of the maxima is solvent dependent, as given in Table 1 and the sample of absorption spectra in 1, 4 dioxane is shown in Figure 2. The emission spectra as shown in Figure 3 show a single peak with a maximum of around 400-410nm for 1MBC with a solvent-dependent peak maximum shift. In comparison to emission spectra, absorption spectra show a smaller shift. Less significant absorbance shift with solvent polarity signifies less distortion in ground state energy distribution which is the fact for less polar molecule in ground state compared to its excited state.

The substantial Stokes shift indicates that the higher state has a different geometry than the ground state. The

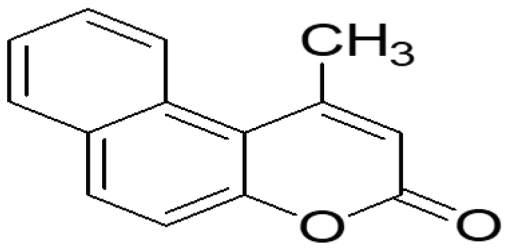


Figure 1. Molecular structure of 1MBC.

molecule shows a standard solvatochromism with more sensitivity for polar solvents in its higher state. This is evident by the stoke shift changes. Further bathochromic shift with increasing solvent polarity in emission peak as seen in Table 1 affirms $\pi \rightarrow \pi^*$ transition.

3.1.2 Dipole Moment of the Excited State

Table 2 sums up the different functions of different solvents. Band shift information from Table 1 was utilised to plot ($\bar{\nu}_a$ - $\bar{\nu}_f$) v/s f(ε, n), ($\bar{\nu}_a$ + $\bar{\nu}_f$) v/s φ(ε, n) charts with slopes m(1) and m(2) separately and are displayed from Figures 4(A) and 4(B). Plots of different functions are given in Figures 5, 6 and 7 with slopes m1, m2 and m3 respectively. Table 3 gives data and analysis pertaining to the graphs which are further assessed utilising the following equations.

$$\mu_g = \frac{m^{(2)} - m^{(1)}}{2}\left[\frac{hca^3}{2m^{(1)}}\right]^{1/2} \quad (1)$$

$$\frac{\mu_e}{\mu_g} = \left[\frac{m^{(2)} + m^{(1)}}{m^{(2)} - m^{(1)}}\right] \quad (2)$$

$$\mu_g = \frac{m_3 - m_2}{2}\left[\frac{hca^3}{2m_2}\right]^{1/2} \quad (3)$$

$$\mu_e = \frac{m_3 + m_2}{2}\left[\frac{hca^3}{2m_2}\right]^{1/2} \quad (4)$$

and for $m_3 > m_2$

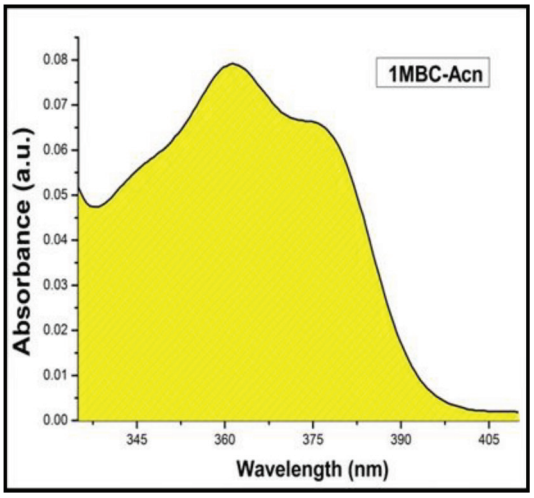


Figure 2. Typical absorption spectrum of 1MBC.

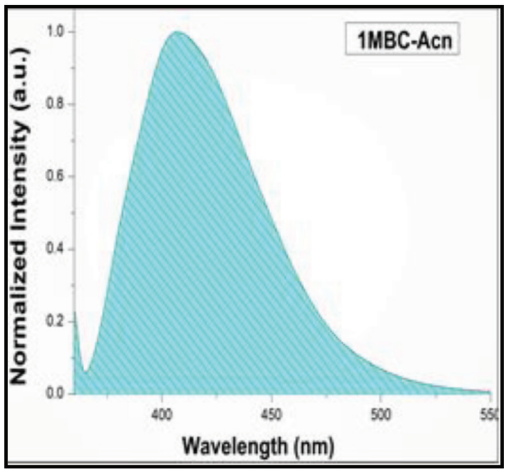


Figure 3. Typical emission spectrum of 1MBC.

Table 1. Photophysical parameters of 1MBC in different solvents

Solvent	λ_a (nm)	λ_f (nm)	$\bar{\nu}_a$ (cm^{-1})	$\bar{\nu}_f$ (cm^{-1})	($\bar{\nu}_a$ - $\bar{\nu}_f$) (cm^{-1})	($\bar{\nu}_a$ +ν_f) (cm^{-1})	½($\bar{\nu}_a$ + $\bar{\nu}_f$) (cm^{-1})
1,4 Dioxane	353.0	400.0	28328.6	25000.0	3328.6	53328.6	26664.3
Toluene	354.0	401.0	28248.6	24937.7	3310.9	53186.2	26593.1
1 Butanol	357.0	408.5	28011.2	24479.8	3531.4	52491.0	26245.5
Isopropanol	356.0	407.0	28089.9	24570.0	3519.9	52659.9	26330.0
1 Propanol	356.5	407.5	28050.5	24539.9	3510.6	52590.4	26295.2
Ethanol	356.0	407.5	28089.9	24539.9	3550.0	52629.8	26314.9
Methanol	357.5	409.5	27972.0	24420.0	3552.0	52392.1	26196.0
Acetonitrile	357.5	409.0	27972.0	24449.9	3522.2	52421.9	26211.0
DMF	358.0	410.5	27933.0	24360.5	3572.4	52293.5	26146.7
DMSO	359.0	410.5	27855.2	24360.5	3494.6	52215.7	26107.8

$$\mu_e = \left[\frac{m_2 + m_3}{m_3 - m_2}\right]\mu_g \quad (5)$$

Here molecular volume is used to determine "a". The above-calculated values are recorded in Table 4.

For unaligned dipole moments, then the angle between them φ can be determined utilizing Eq.(6).

$$\cos\varphi = \frac{1}{2\mu_g\mu_e}\left[\left(\mu_g^{\,2} + \mu_e^{\,2}\right) - \frac{m_3}{m_2}\left(\mu_e^{\,2} - \mu_g^{\,2}\right)\right] \quad (6)$$

With a good correlation coefficient, dipole moment values calculated herewith are recorded in Table 4. A negative value of m_3 is observed here which is already reported by many researchers[11,26].

Ground state and singlet excited energy state dipole minutes are assessed by utilising Equations (1) and (2) where the ground state dipole moment is around 1.86 D ($\mu_g^{\,c}$) while the excited state dipole moment is 3.00D ($\mu_e^{\,d}$). The angle formed by dipoles in their ground (μg) and excited energy state (μe) is determined utilizing Equation (6) to find if they are parallel to one another according to the suppositions in Bilot and Kawski conditions or if they form any angle.

The angle between the dipole minutes is viewed as 0° affirming that both electronic states are parallel to each other. Dipole moment increases on excitation recommended Intra-atomic Charge move (ICT) in an excited energy state where the molecule is turning out to be more polar on excitation. μe value in Table 4 calculated from different methods show insignificant difference. The dipole moment of the excited state turns out to be large, which determines the different excited state geometry to the ground state.

3.1.3 *Molecular Microscopic Solvent Polarity Parameter*

Compared with the conventional approach of using the dielectric constant and refractive index of solvents in the form of functions, Reichardt's proposed empirical solvent parameter (E_T^N), which relates better with the spectral shift. Plots corresponding to (E_T^N) is shown in Figure 8 where the linear graph determines the general solute-solvent interactions. Slope 'm' of the above graph is used to calculate Δμ which is given by Equation (7)

$$\Delta\mu = \left(\mu_e - \mu_g\right) = \sqrt{\frac{\mathrm{mX81}}{\left(6.2/\mathrm{a}\right)^3 11307.6}} \quad (7)$$

E_T^N values of all the solvents are referred from literature[22]. Utilizing E_T^N, calculated excited state dipole moment as μ_e^i determined by Equation. (7). Polarity changes with respect to the lower and higher energy states $\Delta\mu_e^j$ and $\Delta\mu_e^k$ are in Table 4 . The observation of a decent agreement between the Reichardt and Bilot-Kawski approaches lends support to the higher excited state dipole moment. Additionally, the Coumarin derivative exhibits a more polar nature in its excited energy state than in its ground state and has a higher change in dipole moment.

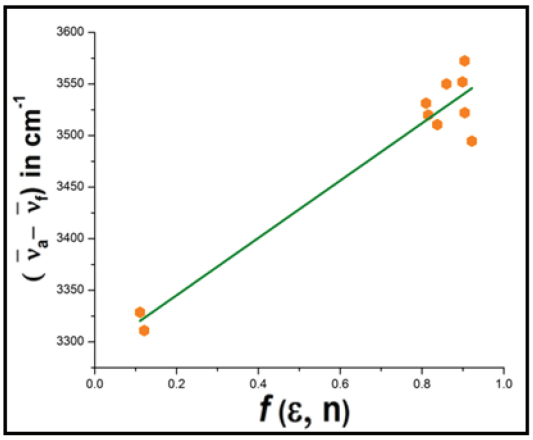


Figure 4(a)

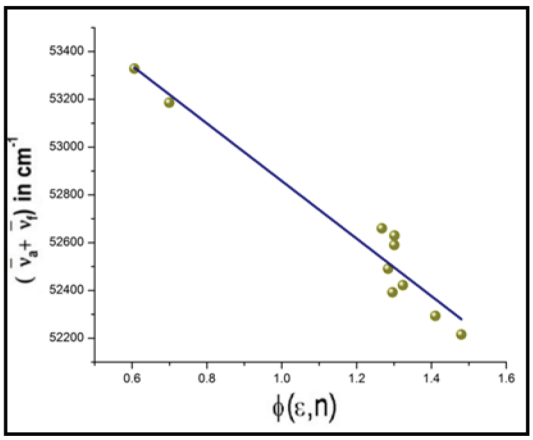


Figure 4(b)

Figure 4. Linear plots of 4(a) f(ε, n) and 4(b) φ(ε, n) of 1MBC using Bilot Kawaski.

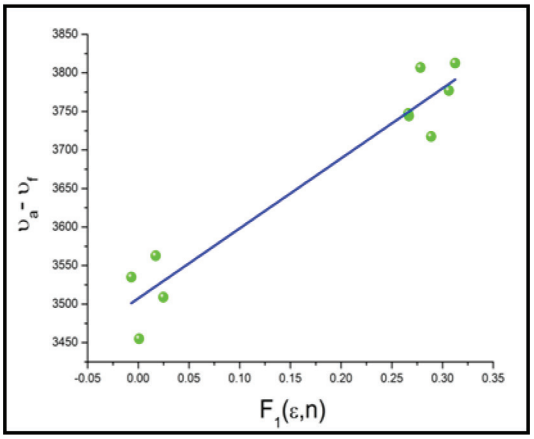


Figure 5. Linear plots of Stoke's shift v/s $F_1(\varepsilon, n)$

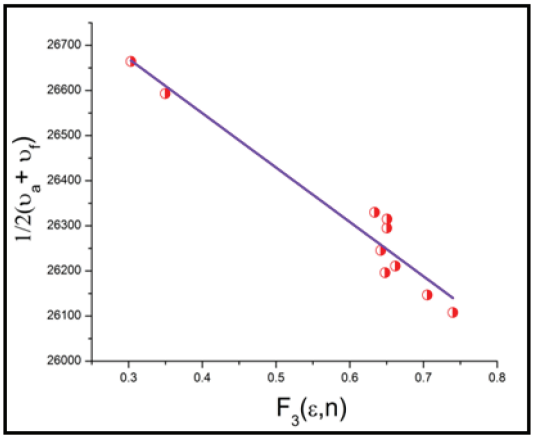


Figure 7. Linear plots of $1/2(\bar{\nu}_a+\bar{\nu}_f)$ v/s F_3 *(ε, n)*.

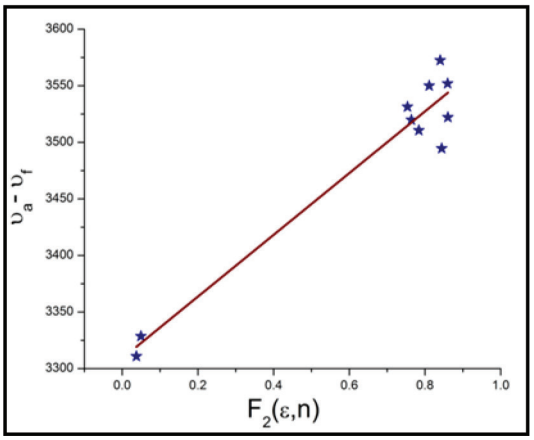


Figure 6. Linear plots of Stoke's shift. v/s $F_2(\varepsilon, n)$.

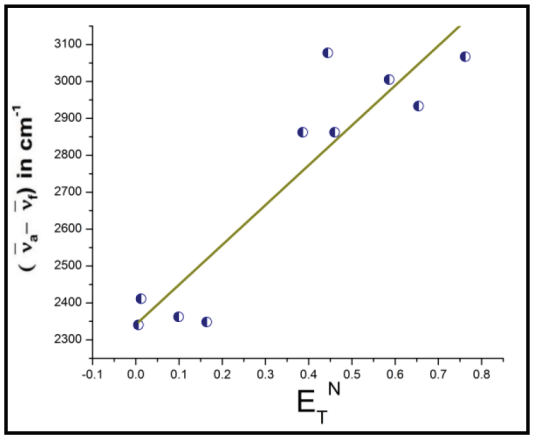


Figure 8. Linear plots of Stokes'shift v/s .

3.2 Quantum Computations

3.2.1 Optimised Structure

DFT/B3LYP/6-31+G(d,p) optimised geometry of the particle is given in Figure 9. Figure 10 shows the gas phase DFT calculated ground state dipole moment with the value 5.87D. Noticed variation in theoretically determined dipole moment in comparison with experimental values is due to the way the theoretical computations are performed on an individual particle in the gaseous state.

3.2.2 Frontier Molecular Orbital Analysis

The energy difference between Highest Occupied Molecular Orbit (HOMO) and Lowest Unoccupied Molecular Orbit (LUMO) provides an energy gap which assumes a significant part in explaining molecular transport properties. FMO estimations are done by DFT/B3LYP. The HOMO-LUMO 3D plots are given in Figure 11. Here HOMO is localised on the Coumarin ring and LUMO is spread through the substituted methyl group along with the Coumarin ring. In 1MBC methoxy acts like an acceptor and charge transfer happens from the donor Coumarin ring to the acceptor Methoxy group.

The more stable the molecule will be if the energy gap is larger, and the molecule is more reactive if the energy gap is small. The following equations show different parameters[27,28], that are obtained using HOMO-LUMO values which helps in understanding the utility of molecules in different applications.

As per Koopmans' theorem, we have[29] the below:

Ionization Potential (IP)-ELUMO

Electron Affinity (EP)=EHOMO

Electronegativity (χ) =1/2 (IP+EA)

Chemical Potential (μ)=1/2 (1P+EA)

Table 2. Dielectric constant (ε), refractive index (n), solvent polarity functions, microscopic solvent polarity parameters (E_T^N)

Solvent	ε	n	E_T^N	$F_1(\varepsilon,n)^a$	$F_2(\varepsilon,n)^b$	$F_3(\varepsilon,n)^c$	$\varphi(\varepsilon,n)^d$	$f(\varepsilon,n)^d$
1,4 Dioxane	2.21	1.4	0.164	0.024682	0.049472	0.303191	0.606383	0.110858
Toluene	2.4	1.4	0.099	0.017104	0.037469	0.349645	0.69929	0.121057
1 Butanol	17.53	1.3	0.586	0.266778	0.753785	0.642037	1.284075	0.809977
Isopropanol	17.9	1.3	0.617	0.274776	0.763988	0.63376	1.26752	0.815148
1 Propanol	20.73	1.3	0.617	0.276601	0.783788	0.650358	1.300716	0.837444
Ethanol	24.13	1.3	0.654	0.288753	0.811143	0.650624	1.301247	0.859851
Methanol	33.61	1.3	0.762	0.312475	0.859689	0.647896	1.295792	0.899042
Acetonitrile	36.01	1.3	0.46	0.306170	0.860593	0.661876	1.323752	0.90453
DMF	37.31	1.4	0.386	0.278209	0.84033	0.705248	1.410496	0.904371
DMSO	47.13	1.4	0.444	0.266113	0.844059	0.739953	1.479905	0.921901

[a] Lippert-Mataga solvent function
[b] Bakhshiev solvent function
[c] Kawski-Chamma-Viallet solvent function
[d] Bilot-Kawski polarity function

Table 3. Statistical treatment of the correlations of solvents spectral shifts of 1MBC

Correlations	Slope		Correlation Factor "r"	Number of Data
Bilot- Kawaski Correlation	$m^{(1)}$	278.0	0.92	10
	$m^{(2)}$	1205.0	0.93	10
Lippert Correlation	m_1	801.5	0.94	10
Bakhshiev's Correlation	m_2	272.8	0.93	10
Kawski-Chamma- Viallet's Correlation	m_3	1205.0	0.93	10
E_T^N Clation	M	361.9	0.67	10

Table 4. Dipole moments of 1MBC

Solute	Radius (A^0)	$\mu_g{}^a$ (D)	$\mu_g{}^b$ (D)	$\mu_g{}^c$ (D)	$\mu_e{}^d$ (D)	$\mu_e{}^e$ (D)	$\mu_e{}^f$ (D)	$\mu_e{}^g$ (D)	$\mu_e{}^h$ (D)	$\mu_e{}^i$ (D)	$\Delta\mu^j$	$\Delta\mu^k$	ϕ^l
1MBC	3.561	5.87	1.86	2.98	1.89	2.99	3.79	3.00	4.22	2.38	1.12	0.49	0°

[a]Dipole moment in the ground state calculated by Gaussian software.
[b]Dipole moment in the ground state calculated using the Bilot-Kawski method.
[c]Dipole moment in the excited state calculated using the Bilot-Kawski method.
[d]Dipole moment in the ground state calculated experimentally.
[e]Dipole moment in the excited state calculated experimentally.
[f]Excited state dipole moment calculated using the Lippert Mataga method.
[excited] state dipole moment calculated using the Bakhshiev method.
[h]Excited state dipole moment calculated using the Kawski-Charnma-Viallet method.
[i]Dipole moment calculated using the E^N_T equation of the Reichardt method.
[change] in dipole moments from the Bilot-Kawski method.
[k]Change in dipole moments calculated from E^N_T parameter.

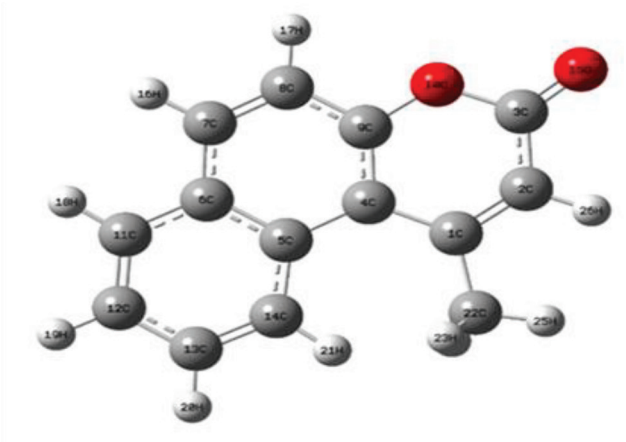


Figure 9. Optimised diagrams of 1MBC.

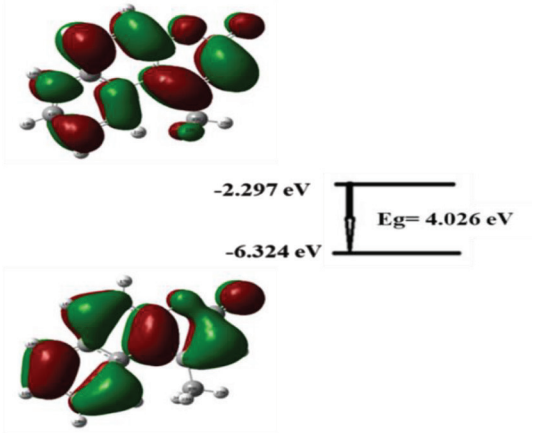


Figure 11. HOMO-LUMO structure of 1MBC.

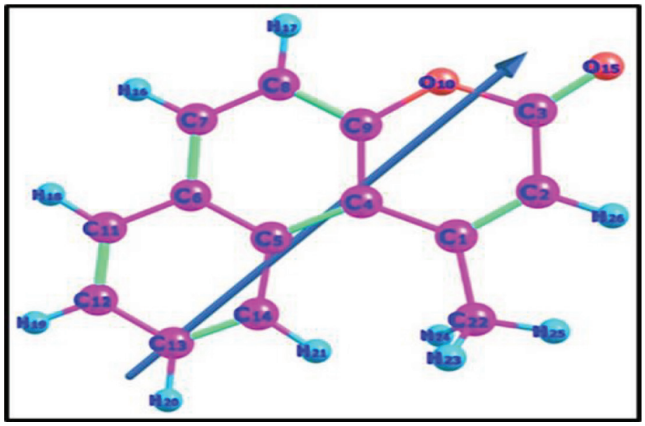


Figure 10. Ground state optimised molecular geometries of 1MBC. The arrow indicates the direction of the dipole moment.

Chemical Hardness (η)=1/2 (1P-EA)
Chemical Softness (S)= 1/ η
Electrophilicity (ω)= $\mu^2/2\eta$

Table 5 gives FMOs and the molecular property values calculated for 1MBC. The energy gap value for 1MBC is found to be 4.026 implying the molecule is more chemically stable. The energy gap of 1MBC is lower, which indicates that the electron density present within the molecules is not localized. This enhances its molecular reactivity. The observed lower electron affinity and higher ionisation potential values of 1MBC allow for the possibility of higher nucleophilic and electrophilic reactions.

3.2.3 MEP Analysis

MEPs represent electronic cloud surfaces which can be used to correspond to reactivity in a compound. The intensities of the electrostatic potential energy changes (for electrophilic and nucleophilic regions) are depicted using red and blue colour codes as the lowest and highest electrostatic potential energy value[29].

The calculated value of MEP and optimised geometry for the compound are mapped and shown in Figure 12. In the case of 1MBC, both electropositive and electro-negative region lies in the Coumarin ring and Methoxy substitution shows the neutral potential with green colour. MEP and contour analysis together display the nucleophilic and electrophilic reaction sites. The contour map on MEP further supports positive and negative regions as depicted by the total electron density surface which is shown in Figure 12.

3.2.4 Mulliken Charges

Charge transfer defines molecular reactivity of molecules and atomic charge analysis is computed using Mulliken studies. B3LYP methods with 6-31+G (d, p) basis level are used for this study where Figure 13 shows the Coumarin derivative's Mulliken charge distribution. Here observation shows that electro-negative atoms N, F and O have negative charges, while all Hydrogen atoms have a positive charge. Carbon atoms with both positive and negative charges in Figure 13 are highly influenced by their substituents and act as a centre for charge transfer. For 1MBC out of a total of 26 atoms, carbon atom C1 of the Coumarin ring has the highest positive charge to which the substituted Methyl group is attached and the C9 carbon atom has the highest negative charge representing charge transfer between the Coumarin ring and the Methoxy group.

Table 5. FMO derived properties values of 1MBC

Molecule	IP	EA	P (eV)	χ(eV)	η (eV)	σ (eV)	ω (eV)
1MBC	6.324	2.297	-4.311	4.311	2.014	0.497	4.614

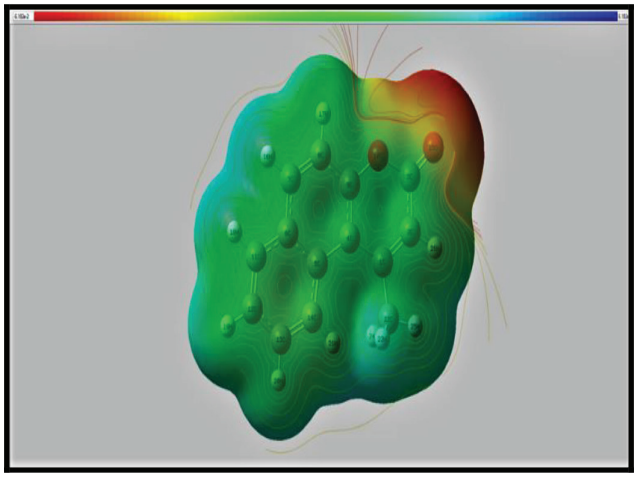


Figure 12. The total electron density mapped with the MEP surface for 1MBC.

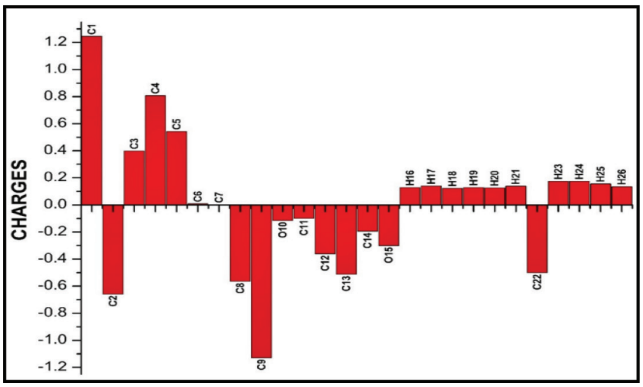


Figure 13. Mulliken charges for 1MBC.

Table 6. NLO properties of 1MBC

	a.u	esu(x10^{-24})		a.u	esu(x10^{-33})
α_{xx}	271.5412	40.2403	β_{xxx}	99.7628	862.2539
α_{xy}	3.922084	0.5812	β_{yxx}	224.2262	1937.9968
α_{yy}	180.3519	26.7267	β_{xyy}	-126.3524	-1092.0688
α_{xz}	0.010925	0.0016	β_{yyy}	-35.8584	-309.9259
α_{yz}	-0.0549	-0.0081	β_{zxx}	0.2176	1.8809
α_{zz}	84.79901	12.5665	β_{xyz}	-0.1319	-1.1401
α_{0}	178.8974	26.5112	β_{zyy}	0.0317	0.2740
Δα	161.7382	23.9683	β_{xzz}	90.3425	780.8341
μ_{x}	2.1693		β_{yzz}	12.5504	108.4738
μ_{y}	0.7928		β_{zzz}	-0.0585	-0.5055
μ_{z}	0.0031		β_{0}	210.79043	1821.8706
μ	2.3096	5.8705 Debye			

3.2.5 NLO

NLO properties finding major applications are correlated with molecular structures[30] with polarisability and hyperpolarisability computation where large hyperpolarisabilities are preferred. α, μ and β_{ijk} were calculated using DFT/B3LYP with 6-31+G (d, p) basis level for the compound.

Calculated values of Polarisabilities and hyperpolarisabilities are found to be 26.5112 and 18.218x10-30 for 1MBC in esu units and are tabulated in Table 6. Computed values of dipole moment for 1MBC are compared with prototypical urea and is found that the value is 1.50 times of urea. Hyperpolarisabilities are found to be 29.218 times greater than urea (β tot = 0.6218 X10^{-30} esu) for 1MBC. This indicates that the study helps to explore in detail nonlinear optical properties and also helps in the design of newer molecules.

3.2.6 NBO Analysis

Intra- and intermolecular bonding explanation, analysis of stability, transfer of charge and conjugative interactions are analysed by NBO analysis tool[31] from Gaussian 9W software. A perturbative calculation leads to bonding and anti-bonding interactions, which are estimated by the NBO method. This method expresses stabilisation energy linked with the delocalisation value of i, j as an estimate of Lewis and Non-Lewis type interactions owing to second-order perturbation theory[32]

The bonding and anti-bonding efficient interactions are calculated and listed in Table 7. As observed from the table we have two types of donors and acceptors pair (σ, π, σ* and π*) and depict the following most probable transitions with the understanding of perturbation energy E2. For 1MBC, hyper-conjugative interactions

Table 7. Bonding and anti-bonding analysis of 1MBC

Donor(i)	E_D(e)	Accepter(j)	E_D(e)	$E_{(2)}$kj/mol	E_j-E_i (a.u.)	$F_{(i,j)}$ (a.u.)
σ(C1-C2)	1.97682	σ*(C11-H18)	0.01403	306.23	0.69	0.411
σ(C1-C22)	1.98213	σ*(C22-H23)	0.00937	28985	0.42	3.128
σ(C4-C9)	1.97218	σ*(C2-H26)	0.01322	13238	0.08	0.943
π(C11-C12)	1.72358	π*(C11-C12)	0.26231	180.49	0.2	0.172
σ(C11-H18)	1.97883	σ*(C22-H23)	0.00937	10791	3.09	5.171
σ(C11-H18)	1.97883	σ*(C22-H24)	0.0094	29374	1.55	6.041
σ(C13-C14)	1.9801	σ*(C22-H23)	0.00937	23017	0.77	3.766
π(C13-C14)	1.72759	σ*(C13-C14)	0.2742	2141.4	2.08	1.883
σ(C22-H23)	1.9742	σ*(C22- H24)	0.0094	29956	1.66	6.313
σ(C22-H24)	1.9741	σ*(C13- H20)	0.01348	24473	5.49	10.379
σ(C22-H24)	1.9741	σ*(C14- H21)	0.01554	39562	4.33	11.711
σ(C22-H24)	1.9741	σ*(C22- H24)	0.0094	12590	9.33	9.713
LP(O10)	1.96318	σ*(C11- H18)	0.01403	265.25	0.72	0.393

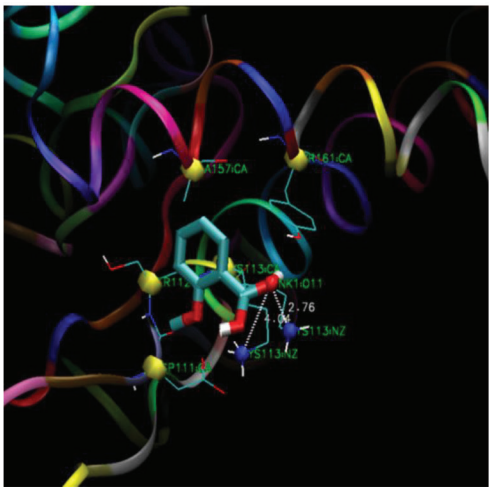


Figure 14. Best affinity mode of docked compound 1MBC with 2-IPM protein.

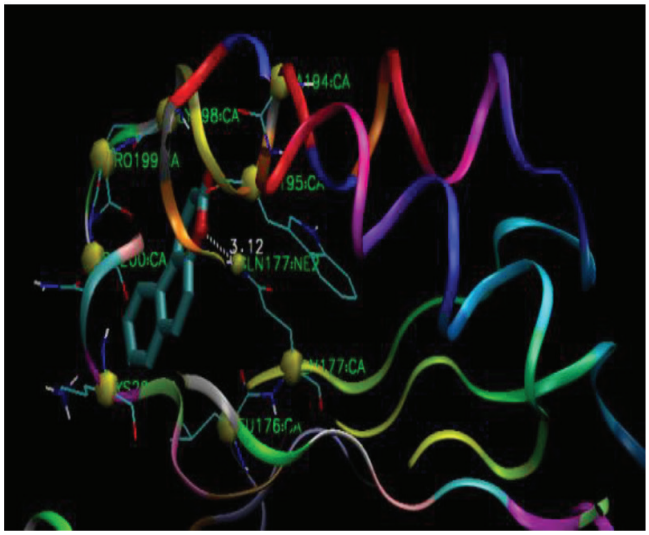


Figure 15. Best affinity mode of docked compound 1MBC with 2-IPL protein.

are of second-order type taking place between lone pairs and σ orbitals or between σ and σ* orbitals. Here probable transition is C22-H24 → C14-H21 (39562.6 kj/mol, σ → σ*), C22-H23 → C22-H24 (29956.6 kj/mol, σ → σ*), C11-H18 → C22-H24 (29374.2.6 kj/mol, σ → σ*), C1-C22 → C22-H23 (28985.2 kj/mol, σ → σ*). These transitions are leading to the stabilisation of 1MBC. Also, an important role in the formation of bonds in Coumarin molecules is played by nitrogen and oxygen atoms having Lone Pair (LP). In 1MBC lone pair interactions are mainly O10 (σ) to C11-H18 (σ*) (265.2 kj/mol).

3.2.7 Molecular Docking Studies

Docking preparation and pre-processing were performed by using VMD 1.9.3 and the crystal structure of galactose binding periplasmic proteins (PDB ID: 2IPM and 2IPL) was retrieved from the protein data bank. The molecular docking for 1MBC was carried out using 1.5.6 version Auto Dock Tools software using VMD and is shown in Figures 14 and 15. The docking energy profile and interactions with amino acid residues are shown in Table 8.

Table 8. Interaction of 2IPM and 2IPL protein for 1MBC with docked energy parameters

Docked Energy Parameters	2IPM	2IPL
Binding_Energy (kcal/mol)	-8.55	-8.59
Ligand_Efficiency	-0.53	-0.54
Inhib_Constant	543.26 (nM)	506.26 (nM)
Intermol_Energy (kcal/mol)	-8.55	-8.59
Electrostatic Energy (kcal/mol)	-0.01	0.03
Total_Internal Energy. (kcal/mol)	0.0	0.0
Torsional_Energy. (kcal/mol)	0.0	0.0
Unbound_Energy (kcal/mol)	0.0	0.0
Hydrogen Bonds	No hydrogen bonding interactions	GLN177, LEU36
Interaction with Amino acids within 3.5 A' of Ligand	LEU176, GLN177, ALA194, TRP195, GLY198, PRO199, ASN200, LYS203	GLU25, ALA28, VAL34, GLN35, LEU36, MET38

4.0 Conclusions

Theoretical and experimental analysis of heterocyclic compound 1MBC has been carried out in detail. From all types of solvatochromic approaches dipole moment calculated for the test molecule is greater in the excited energy state than in the ground state. Although dipole moments are found to be less Δμ varaition is very prominent. This illustrates coumarin derivatives to have large charge distribution and more polar nature in excited state than in ground states. Also, an increase in the polarity of the solvent causes a red shift in the stokes line. This confirms $\pi \rightarrow \pi^*$ the transition for both the molecules together with the ICT character. This helps develop a better understanding of coumarin derivatives based on their structure composition for different NLO, sensors, dye lasers and different applications. MEP analysis of 1MBC shows both +ve and -ve potential surfaces are centred at the Coumarin ring. Local and global parameters are analysed from Frontier Molecular Orbital analysis which shows 1MBC having good chemical stability and strength. The NLO properties of test molecules were analysed by comparing their first hyperpolarisabilities with those of the prototypical NLO materials and confirmed that 1MBC is found to be very active. The docking analysis indicated that at active sites, compound 1MBC exhibited the most favourable binding pattern, forming non-covalent interactions with amino acid residues of the proteins. Utilisation of coumarin derivatives in the field of mining industry is still under development, these industries stand to benefit greatly from their potential. Because of their special qualities, they are useful instruments for raising productivity, cutting expenses and safeguarding the environment.

5.0 Acknowledgements

The authors are thankful for the grant (GRD no: 1106/2021-22/ 491) from the Department of Science and Technology (DST), Government of India and Vision Group of Science and Technology (VGST), Govt. of Karnataka which helped in setting up a computational workstation.

6.0 References

1. Oliveira E, Bértolo E, Núñez C, Pilla V, Santos HM, Fernández-Lodeiro J, Fernández-Lodeiro A, Djafari J, Capelo JL, Lodeiro C. Green and red fluorescent dyes for translational applications in imaging and sensing analytes: A dual-color flag. ChemistryOpen. 2018; 7(1):9-52. https://doi.org/10.1002/open.201700135 PMid:29318095 PMCid: PMC5754553.
2. Zeng X, Chen X, Chen J, Ma M, Jin H, Yu S, Liu Z. A simple highly selective ratiometric fluorescent probe for detection of peroxynitrite and its bioimaging applications. Dyes Pigm. 2023; 210:110993. https://doi.org/10.1016/j.dyepig.2022.110993
3. Bassan E, Gualandi A, Cozzi PG, Ceroni P. Design of BODIPY dyes as triplet photosensitisers: Electronic properties tailored for solar energy conversion, photoredox catalysis and photodynamic therapy. Chem Sci. 2021; 12(19):6607-28. https://doi.org/10.1039/D1SC00732G PMid:34040736 PMCid: PMC8132938.
4. Singh P, Jaiswal S, Kushwaha A, Gahlowt P, Mishra V, Tripathi DK, Singh SP, Gupta R, Singh VP. Peroxynitrite

is essential for aerenchyma formation in rice roots under waterlogging conditions. Planta. 2023; 258(1):2. https://doi.org/10.1007/s00425-023-04148-6 PMid:37208534.
5. Papadopoulos J, Mueller TJ. Rapid synthesis of 4-alkynyl coumarins and tunable electronic properties of emission solvatochromic fluorophores. Dyes Pigm. 2019; 166:357-66. https://doi.org/10.1016/j.dyepig.2019.03.038
6. Elaryian HM, Bedair MA, Bedair AH, Aboushahba RM, Fouda AE. Synthesis, characterization of novel coumarin dyes as corrosion inhibitors for mild steel in acidic environment: Experimental, theoretical, and biological studies. J Mol Liq. 2022; 346:118310. https://doi.org/10.1016/j.molliq.2021.118310
7. Kajiwara K, Osaki H, Greßies S, Kuwata K, Kim JH, Gensch T, Sato Y, Glorius F, Yamaguchi S, Taki M. A negative-solvatochromic fluorescent probe for visualizing intracellular distributions of fatty acid metabolites. Nat Commun. 2022; 13(1):2533. https://doi.org/10.1038/s41467-022-30153-6 PMid:35534485 PMCid: PMC9085894.
8. Howe ME, Garcia-Garibay MA. Fluorescence and rotational dynamics of a crystalline molecular rotor featuring an aggregation-induced emission fluorophore. The Journal of Org Chem. 2019; 84(15):9570-6. https://doi.org/10.1021/acs.joc.9b01201 PMid:31288516.
9. Sharma K, Melavanki R, Muttannavar VT, Bhavya P, Meghana U, Suma B. Fluorescence spectroscopic studies on preferential solvation and bimolecular quenching reactions of Quinolin-8-ol in binary solvent mixtures. Journal of Physics: Conference Series 2020; 1473(1):012045. IOP Publishing. https://doi.org/10.1088/1742-6596/1473/1/012045
10. Bhavya P, Melavanki R, Kusanur R, Sharma K, Muttannavar VT, Naik LR. Effect of viscosity and dielectric constant variation on fractional fluorescence quenching analysis of coumarin dye in binary solvent mixtures. Luminescence. 2018; 33(5):933-40. https://doi.org/10.1002/bio.3492 PMid:29745063.
11. Bhavya P, Melavanki R, Sharma K, Kusanur R, Patil NR, Thipperudrappa J. Exploring the spectral features and quantum chemical computations of a novel biologically active heterocyclic class of compound 2MEFPBA dye: Experimental and theoretical approach. Chem Data Coll. 2019; 19:100182. https://doi.org/10.1016/j.cdc.2019.100182
12. Muddapur GV, Melavanki R, Sharma K, Srinivasa HT, Thipperudrappa J, Patil NR. Fluorescence properties of aromatic asymmetric di-ketone compound in polar and non-polar solvents. Journal of Physics: Conference Series 2020; 1473(1):012044. IOP Publishing. https://doi.org/10.1088/1742-6596/1473/1/012044
13. Kara Zaitri L, Mekelleche SM. Computational study of linear and nonlinear optical properties of substituted thiophene imino dyes using long-range corrected hybrid DFT methods. Mol Phys. 2020; 118(4):1618508. https://doi.org/10.1080/00268976.2019.1618508
14. Frau J, Glossman-Mitnik D. Conceptual DFT study of the local chemical reactivity of the dilysyldipyrrolones A and B intermediate melanoidins. Theor Chem Acc. 2018; 137(5):67. https://doi.org/10.1007/s00214-018-2244-x
15. Flores-Holguín N, Frau J, Glossman-Mitnik D. Computational chemistry and molecular modelling techniques for the study of Micropeptin EI-964: Insights into its chemical reactivity and potential pharmaceutical properties. Comput Mol Biosci. 2023; 13(3):35-47. https://doi.org/10.4236/cmb.2023.133003
16. Kusanur RA, Kulkarni MV. A novel route for the synthesis of racemic 4-(Coumaryl) alanines and their antimicrobial activity. Asian J Chem. 2014; 26(4):1077. https://doi.org/10.14233/ajchem.2014.15865
17. Sharma K, Melavanki R, Yallur BC, Kusanur R, Patil NR, Shelar VM, Singh D, Rosario J, Hussaini Q, Thampan AV. Optical characterization of chalcone-doped PMMA thin films for photonic applications using spectroscopic technique of drop casting method. InMacromolecular Symposia 2020; 392(1):2000165). https://doi.org/10.1002/masy.202000165
18. Bilot L, Kawski A. Zur Theorie des Einflusses von Lösungsmitteln auf die Elektronenspektren der Moleküle. Z Naturforsch A. 1962; 17(7):621-7. https://doi.org/10.1515/zna-1962-0713
19. Bilot L, Kawski A. Dipolmomente einiger Phthalimid-Derivate im ersten angeregten Singulettzustand. Z Naturforsch A. 1963; 18(2):256-6. https://doi.org/10.1515/zna-1963-0228
20. Lippert E. Spectroscopic determination of the dipole moment of aromatic compounds in the first excited singlet state. Z Elektrochem. 1957; 61(8):962-75. https://doi.org/10.1002/bbpc.19570610819
21. Bakhshiev NG. Universal intermolecular interactions and their effect on the position of the electronic spectra of molecules in 2-component solutions. 7. Theory (general case for isotopic solution). Opt Spektrosc. 1964; 16(5):821-32.
22. Reichardt C. Solvatochromic dyes as solvent polarity indicators. Chem Rev. 1994; 94(8):2319-58. https://doi.org/10.1021/cr00032a005
23. Melavanki R, Sharma K, Muttannavar VT, Kusanur R, Katagi K, Patra SM, Umapathy S, Sadasivuni KK, Shelar VM, Singh D, Patil NR. Quantum chemical computations, fluorescence spectral features and molecular docking of two biologically active heterocyclic class of compounds. J Photochem Photobiol A: Chemistry. 2021; 404:112956. https://doi.org/10.1016/j.jphotochem.2020.112956
24. Dennington R, Keith T, Millam J, Eppinnett K, Hovell WL, Gilliland R. GaussView, Version 3.09, Semichem. Inc., Shawnee Mission, KS. 2003; 2(1). https://scholar.google.co.in/scholar?hl=en&as_sdt=0%2C5&q=Dennington+et+al.%2C+2003&btn
25. Glendening ED, Weinhold F. Natural resonance theory: II. Natural bond order and valency. J Comput Chem.

1998; 19(6):610-27. https://doi.org/10.1002/(SICI)1096-987X(19980430)19:6<610::AID-JCC4>3.0.CO;2-U

26. Muddapur GV, Melavanki RM, Patil PG, Nagaraja D, Patil NR. Photophysical properties of 3MPBA: Evaluation and co-relation between solvatochromism and quantum yield in different solvents. J Mol Liq. 2016; 224:201-10. https://doi.org/10.1016/j.molliq.2016.09.102
27. Atilgan AB, Yurdakul ŞE, Erdogdu Y, Güllüoğlu MT. DFT simulation, quantum chemical electronic structure, spectroscopic and structure-activity investigations of 4-acetylpyridine. J Mol Struct. 2018; 1161:55-65. https://doi.org/10.1016/j.molstruc.2018.01.080
28. Mohan B, Choudhary M, Bharti S, Jana A, Das N, Muhammad S, Al-Sehemi AG, Kumar S. Syntheses, characterizations, crystal structures and efficient NLO applications of new organic compounds bearing 2-methoxy-4-nitrobenzeneamine moiety and copper (II) complex of (E)-N'-(3, 5-dichloro-2-hydroxybenzylidene) benzohydrazide. J Mol Struct. 2019; 1190:54-67.
29. Lakshminarayanan S, Jeyasingh V, Murugesan K, Selvapalam N, Dass G. Molecular electrostatic potential (MEP) surface analysis of chemo sensors: An extra supporting hand for strength, selectivity & non-traditional interactions. J Photochem Photobiol. 2021; 6:100022. https://doi.org/10.1016/j.jpap.2021.100022
30. George M, Balaji J, Sajan D, Dominic P, Philip R, Vinitha G. Synthesis and third-order optical nonlinearity studies of toluidine tartrate single crystal supported by photophysical characterization and vibrational spectral analysis. J Photochem Photobiol A: Chemistry. 2020; 393:112413. https://doi.org/10.1016/j.jphotochem.2020.112413
31. Frisch A. Gaussian 09W Reference. Wallingford, USA, 25p. 2009;470. https://www.chemistry4.me/Gaussian/G09W/help/g09w_ref.pdf
32. Yeliz UL. Natural bond orbital (NBO) population analysis and non-linear optical (NLO) properties of 2-(azepan-1-yl (naphthalen-1-yl) methyl) phenol. International J Chemi Technol. 2020; 4(2):138-45. https://doi.org/10.32571/ijct.751001